J Mol Model (2003) 9:39–46
DOI 10.1007/s00894-002-0107-8

ORIGINAL PAPER

**Miroslav Pospíšil · Pavla Čapková
Helena Weissmannová · Zdeněk Klika
Miroslava Trchová · Marta Chmielová
Zdeněk Weiss**

Structure analysis of montmorillonite intercalated with rhodamine B: modeling and experiment

Published online: 14 January 2003

Abstract The intercalation process and the structure of montmorillonite intercalated with [rhodamine B]$^+$ cations have been investigated using molecular modeling (molecular mechanics and molecular dynamics simulations), X-ray powder diffraction and IR spectroscopy. The structure of the intercalate depends strongly on the concentration of rhodamine B in the intercalation solution. The presence of two phases in the intercalated structure was revealed by modeling and X-ray powder diffraction: (i) phase with basal spacing 18 Å and with bilayer arrangement of guests and (ii) phase with average basal spacing 23 Å and with monolayer arrangement of guests. In both phases the monomeric and dimeric arrangement can coexist in the interlayer space. Three types of dimers in the interlayer structure have been found by modeling: (i) H-dimer (head-to-head arrangement) present in the 18 Å phase, (ii) sandwich type of the head-to-tail arrangement (present in the 23 Å phase) and (iii) J-dimer (head-to-tail arrangement) present in the 23 Å phase.

Keywords Montmorillonite · Intercalate · Rhodamine B · Molecular mechanics · Molecular dynamics

Introduction

Clay minerals represent very attractive matrices for the intercalation of dye molecules. When, for example, rhodamine is intercalated into the clay, which is transparent in the UV–visible region, it appears to be more thermally stable and to exhibit more efficient luminescence. [1] The intercalation of xanthene dyes in smectite-type clays is followed by changes observed in the absorption spectrum (the so-called metachromatic effect), whereby the main absorption band is shifted to higher energies. [1, 2, 3] This effect is explained by: (i) the interaction between the aluminosilicate layers and the dye (i.e. the interaction between the electron lone pairs of clay surface oxygens and the dye π-system) and (ii) the interaction between the dye molecules in the interlayer space of the clay structure (i.e. dimerization and the π–π interaction between two monomers in the dimer). Rhodamine dyes are considered good probe molecules for studying the clay–dye complexes, as they can be intercalated into the clay structure easily via a cation-exchange mechanism and their photophysics depends on the environmental factors.

In recent years, the photophysics of clay-intercalated xanthene dyes has been studied intensively. [3, 4, 5, 6, 7, 8, 9] In previous studies of the clay–dye complexes, the arrangement of guest molecules in the interlayer space was suggested on the basis of steric considerations and X-ray diffraction measurements. [1, 5, 9, 10, 11, 12, 13] Our present work deals with a structure analysis of montmorillonite intercalated with rhodamine B. It is well known that structure analysis based on the diffraction method is extremely difficult in the case of intercalated clays, especially those of the smectite group, due to the turbostratic disorder of their structures. In such a case, molecular modeling using empirical force fields is a very powerful tool in the investigation of the interlamellar structure. An atomistic computer modeling study of the interlamellar structure in dye–clay complexes was carried out by Breu et al. in [14, 15]. In the present work, we use molecular mechanics and classical molecular dynamics in the *Cerius*^{2} modeling environment [16] combined with X-ray powder diffraction and IR spectroscopy to investigate the arrangement and conformation of [rhodamine B]$^+$ cations in the interlayer space of montmorillonite. The presence of water molecules in the interlayer structure was taken into account in the present calculations. As a result of modeling, we obtain a

M. Pospíšil (✉) · P. Čapková · M. Trchová
Faculty of Mathematics and Physics,
Charles University Prague,
Ke Karlovu 3, 12116 Prague 2, Czech Republic
e-mail: pospisil@karlov.mff.cuni.cz

H. Weissmannová · Z. Klika · M. Chmielová · Z. Weiss
Institute of Materials Chemistry, Technical University Ostrava,
70833 Ostrava-Poruba, Czech Republic

detailed structural model including characterization of the disorder and possible conformational changes. In addition to conventional diffraction analysis, we obtain energy characteristics such as the total sublimation energy and its components (van der Waals, electrostatic, H-bond).

Experiment

Sample preparation and chemical analysis

The montmorillonite samples fully intercalated with rhodamine B were prepared using SWy (montmorillonite, Crook County, Wyoming) and rhodamine B (Fluka Standard Chemika) that was recrystallized twice from deionized water. A saturated sodium form of SWy was prepared from the SWy fraction with grain size less than 5 μm by repeated saturation with 1 mol dm^{-3} NaCl solution. After each step, the sample was centrifuged and a fresh portion of NaCl solution was added. The fully saturated Na form of SWy was then washed out with deionized water and air dried. The montmorillonite samples fully intercalated with rhodamine B were prepared by a similar technique. For the preparation of individual fully saturated samples, rhodamine B solutions of concentration ranging from 1.1×10^{-4} to 4.00×10^{-3} mol dm^{-3} were used (see also Table 1). The saturation was repeated several times until the Na form of SWy was fully intercalated. In each saturation step, the amount of intercalated dyes was determined from the difference between the total rhodamine B concentration before and after saturation. In order to determine the total rhodamine B concentration (monomer and dimer), the solutions were diluted to an approximate concentration of 10^{-5} mol dm^{-3} so that only monomer forms of rhodamine B were present. The total concentrations of rhodamine B solutions were then determined by photometric methods at a wavelength of 552 nm. The correctness of the calculated total amount of intercalated rhodamine B (Table 1) was also checked through the content of C, H, N and O belonging to the rhodamine B cations present in intercalated Swy determined by elemental analysis.

X-ray diffraction measurements

The powder diffraction data for the series of rhodamine B–montmorillonite samples prepared using intercalation solutions with various guest concentrations were collected in the 2θ range 1–10°. An INEL X-ray powder diffractometer with a PSD 120 position sensitive detector was used and the measurements were carried out under the following conditions: the reflection mode, rotating sample holder (capillary) and Cu $K_{K\alpha1}$ radiation. A mixture of silicon and Ag-behenate was used as a calibration standard for the PSD. The results of the powder diffraction analysis are summarized in Table 1, where one can see the effect of the rhodamine B concentration in the intercalation solution on the basal spacing d_{001} and on the interlayer structure of the intercalate. As one can see from Table 1, low concentrations of the intercalation solution lead to two broad diffraction maxima corresponding to basal spacings of about 23 Å and 18–19 Å. Two examples of the diffraction pattern are shown in Fig. 1a, b for samples 1 and 7 (see Table 1). This result suggests the existence of two phases of the intercalated structure for intercalation solutions with low guest concentration. On the other hand, intercalation solutions with a high guest concentration lead to a monophase composition of intercalate with one d_{001} diffraction line at ~18.1 Å. These results support the hypothesis of monomeric and dimeric arrangements of the rhodamine B in the intercalated structure, depending on the concentration of the intercalation solution. [3] The large broadening and slight peak shift of the diffraction lines will be discussed later together with the modeling results.

IR spectroscopic measurements

The structural and optical properties of the samples were checked using Fourier transform infrared (FTIR) spectroscopy. Infrared spectroscopic measurements were performed on a Nicolet IMPACT 400 FTIR spectrometer in an H_2O-purged environment. All spectra in the range 400–4000 cm^{-1} with 2-cm^{-1} spectral resolution were obtained from compressed KBr pellets in which the samples were evenly dispersed. Two hundred scans were used to record each FTIR spectrum. The spectra were corrected for the H_2O and CO_2 content in the optical path. The measured IR spectra for the host structure, guest compound and intercalate (sample 7) are shown in Fig. 2. The strategy of modeling and structure analysis is based on comparison of IR spectra for: (i) the host structure Na-montmorillonite, (ii) the guest compound rhodamine B chloride and (iii) the intercalate rhodamine B–montmorillonite. By comparing these three spectra, we obtain information about possible changes in conformation of the guest molecules and about the bonding geometry of the host layers during intercalation.

Modeling strategy

The initial model for the montmorillonite layer was built using structural data published by Tsipursky and Drits (1984): [17] space group, *C2/m*. The unit cell parameters according to Méring (1967) [18] were used to define the planar unit cell dimensions: a=5.208 Å and b=9.020 Å. The composition of montmorillonite layer according to chemical analysis was $(Al_{1.53}Mg_{0.23}Fe^{3+}_{0.25})(Si_{3.89}Al_{0.10}Ti_{0.01})O_{10}(OH)_2$. To create a supercell of reasonable size for the calculations, the structure formula was modi-

Table 1 Concentration of the rhodamine B in the intercalation solution and corresponding values of the guest concentration in the montmorillonite with the basal spacing detected in the diffraction pattern

Sample No.	Concentration of rhodamine B in the intercalation solution (mol dm^{-3})	Amount of rhodamine B absorbed in montmorillonite (mmol g^{-1})	Basal spacings obtained from the X-ray diffraction pattern d_{001} (Å)	
			First maximum	Second maximum
1	0.00011	0.7060	23.2	18.8
2	0.00046	0.7790	22.9	18.7
3	0.00102	0.7910	21.5	18.7
4	0.00110	0.7960	21.0	18.3
5	0.00370	0.8939	19.7	
6	0.00400	0.8981	18.6	
7	0.00399	0.9045	18.1	

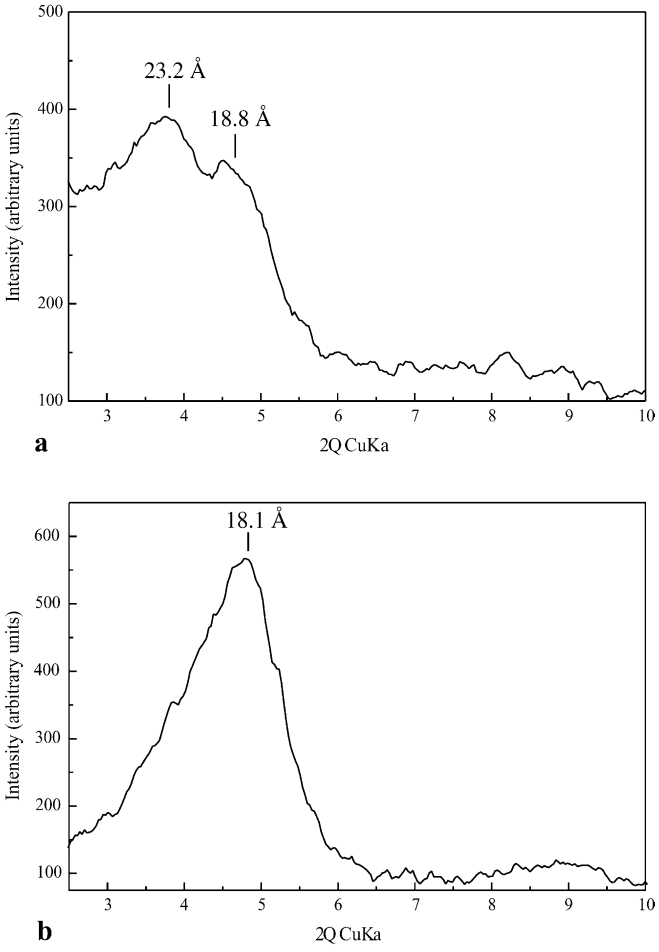

Fig. 1 **a** X-ray powder diffraction pattern of the sample 1, prepared in intercalation solution with the lowest guest concentration (see Table 1). **b** X-ray powder diffraction pattern of the sample 7, prepared in the intercalation solution with the highest guest concentration, according to Table 1

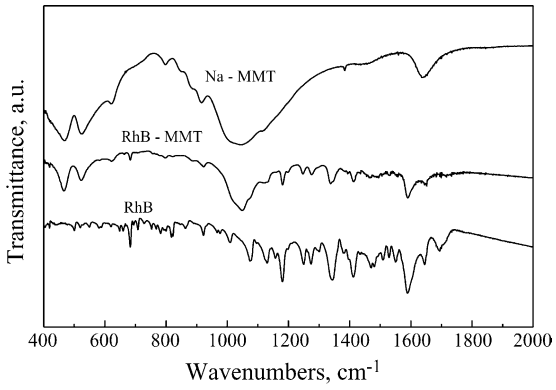

Fig. 2 IR spectra of the host structure Na-montmorillonite (*upper* spectrum), rhodamine B chloride (the *lowest* spectrum) and the intercalate RhB–montmorillonite (the *middle* spectrum)

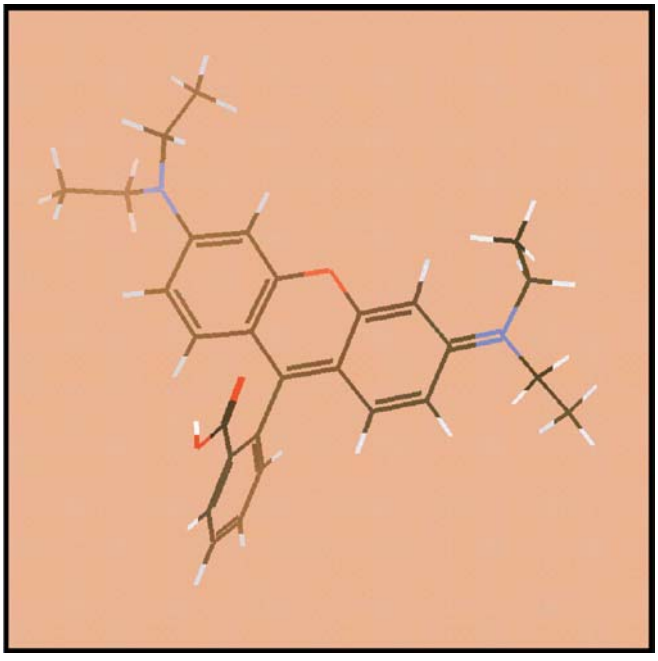

Fig. 3 The rhodamine B cation minimized in vacuum using the universal force field [21]

fied slightly. Consequently, the supercell $3a \times 2b \times 1c$ with layer composition $(Al_{18}Mg_3Fe^{3+}{}_3)(Si_{47}Al_1)O_{120}(OH)_{24}$ was built with a total negative layer charge of −4. The *c* values in the initial model were set up according to the basal spacings obtained from X-ray powder diffraction for samples prepared under different conditions, allowing the replacement of the Na^+ cations by [rhodamine B]$^+$ cations in the interlayer space.

As the intercalation of [rhodamine B]$^+$ into montmorillonite is based on an ion exchange reaction, the host–guest interaction is of a non-bonded nature. This is an important assumption for the modeling strategy. Comparing the IR spectra for the host structure Na-montmorillonite and intercalate in Fig. 2, one can see that the main bands corresponding to the silicate layers are preserved in the spectrum of the intercalate and, consequently, the silicate layers can be treated as rigid bodies during energy minimization. Comparing the IR spectrum of the guest compound rhodamine B chloride with the spectrum of the intercalate, one can see the smoothing and broadening of the vibration bands of [rhodamine B]$^+$ in the intercalated structure. These changes are especially pronounced for bands corresponding to the carboxyl group, skeletal vibrations of the aromatic rings and bending of the ring C–H bonds. (For more details see the next paragraph.) Consequently, the coordinates of all atoms in the [rhodamine B]$^+$ cations were varied during energy minimization, which was performed under the following conditions: variable supercell parameters *c*, α, β and fixed *a*, *b*, γ and with variable bonding geometry and variable position of the [rhodamine B]$^+$ cations. The Ewald summation method was used to calculate the Coulomb energy in a crystal structure. [19] The Ewald sum constant was 0.5 $Å^{-1}$. The minimum charge taken into the Ewald sum was 0.00001e. All atom pairs with separations less than 10 Å were included in the real-space part of the Ewald sum and all reciprocal-lattice vectors with lengths less than 0.5 $Å^{-1}$ were included in the reciprocal part of the Ewald summation. Charges in the crystal are calculated in *Cerius*^{2} using the QEq method (charge equilibrium approach [20]). For the van der Waals energy (VDW) we used the well-known Lennard-Jones functional form, with the arithmetical radius combination rule. The non-bond cut-off distance for the VDW interactions was 7.0 Å.

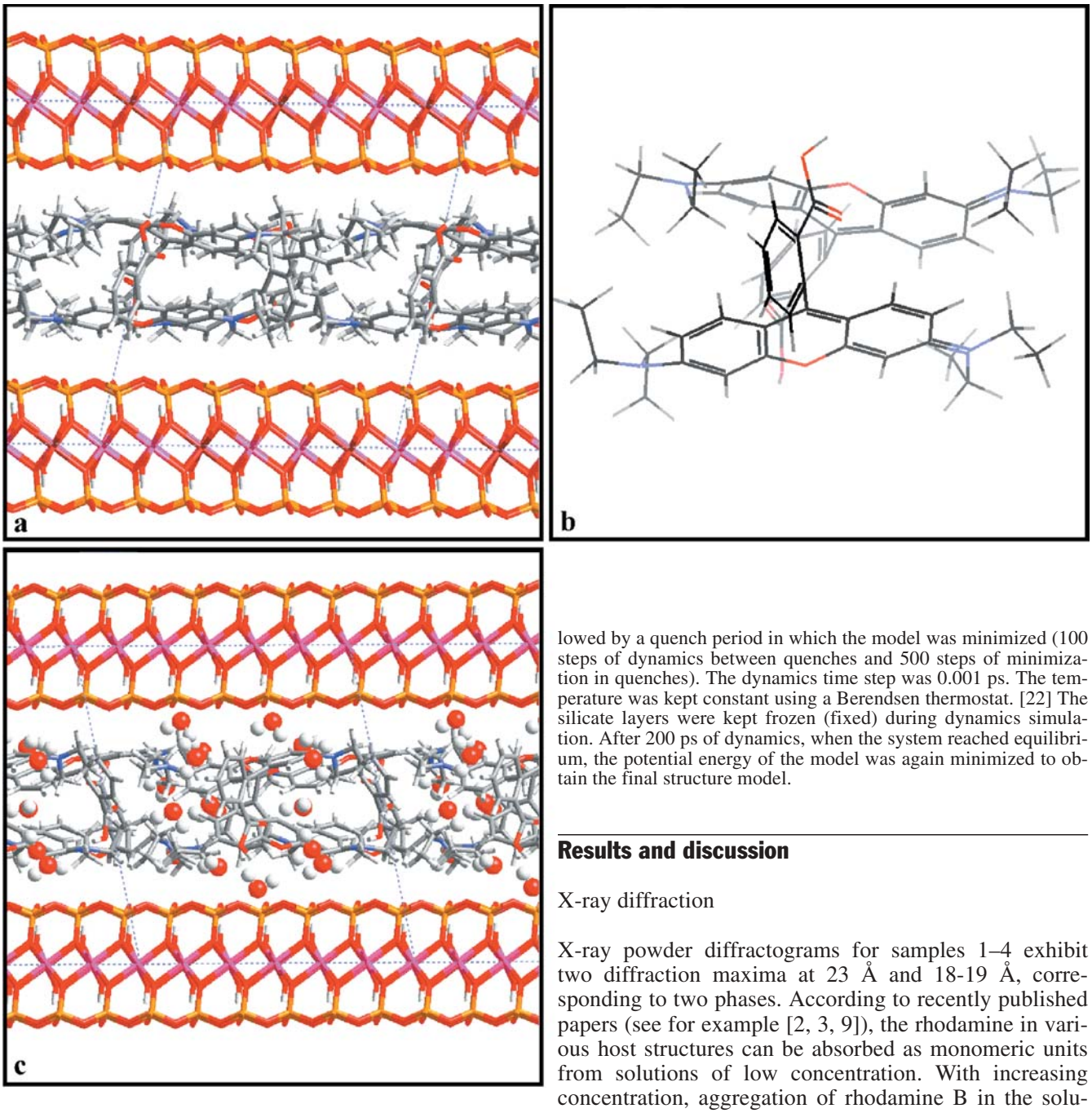

Fig. 4 **a** A side view of the intercalated structure of the phase 18 Å with H-dimeric arrangement, without interlayer water. **b** Detailed view of the H-dimer. **c** Side view of the H-dimeric structure of the phase 18 Å with interlayer water (model 4 in Table 2, with 16 water molecules per 3*a*×2*b*×1*c* supercell

Molecular mechanics calculations and classical dynamic simulations were performed in the *Cerius*^{2} modeling environment. The Universal force field [21] was used to describe the potential energy of initial models. After the first energy minimization in the *Minimizer* module in *Cerius*^{2}, molecular dynamic simulations were started. Quench dynamics was used in an NVT ensemble (constant number of atoms, volume and temperature) at T=300 K. In the quench dynamics, periods of dynamic simulations were followed by a quench period in which the model was minimized (100 steps of dynamics between quenches and 500 steps of minimization in quenches). The dynamics time step was 0.001 ps. The temperature was kept constant using a Berendsen thermostat. [22] The silicate layers were kept frozen (fixed) during dynamics simulation. After 200 ps of dynamics, when the system reached equilibrium, the potential energy of the model was again minimized to obtain the final structure model.

Results and discussion

X-ray diffraction

X-ray powder diffractograms for samples 1–4 exhibit two diffraction maxima at 23 Å and 18-19 Å, corresponding to two phases. According to recently published papers (see for example [2, 3, 9]), the rhodamine in various host structures can be absorbed as monomeric units from solutions of low concentration. With increasing concentration, aggregation of rhodamine B in the solution can be observed and consequently, monomeric and dimeric arrangements can coexist in the intercalated structure. According to this assumption, the dimeric arrangement exhibits the 18.1 Å basal spacing, while the dominant monomeric arrangement leads to the 22–23 Å basal spacing. The large broadening of the diffraction profile, especially for those peaks corresponding to the monomeric phase for the samples 1–4, indicates a high degree of disorder in the interlayer space accompanied by considerable mechanical strain. When discussing the diffraction line broadening, one must also take the Hendricks–Teller effect into account. [23] This is due to the irregular mixing of two interlamellar distances 18.1 Å and ~23 Å, which occurs at the phase boundaries. As a

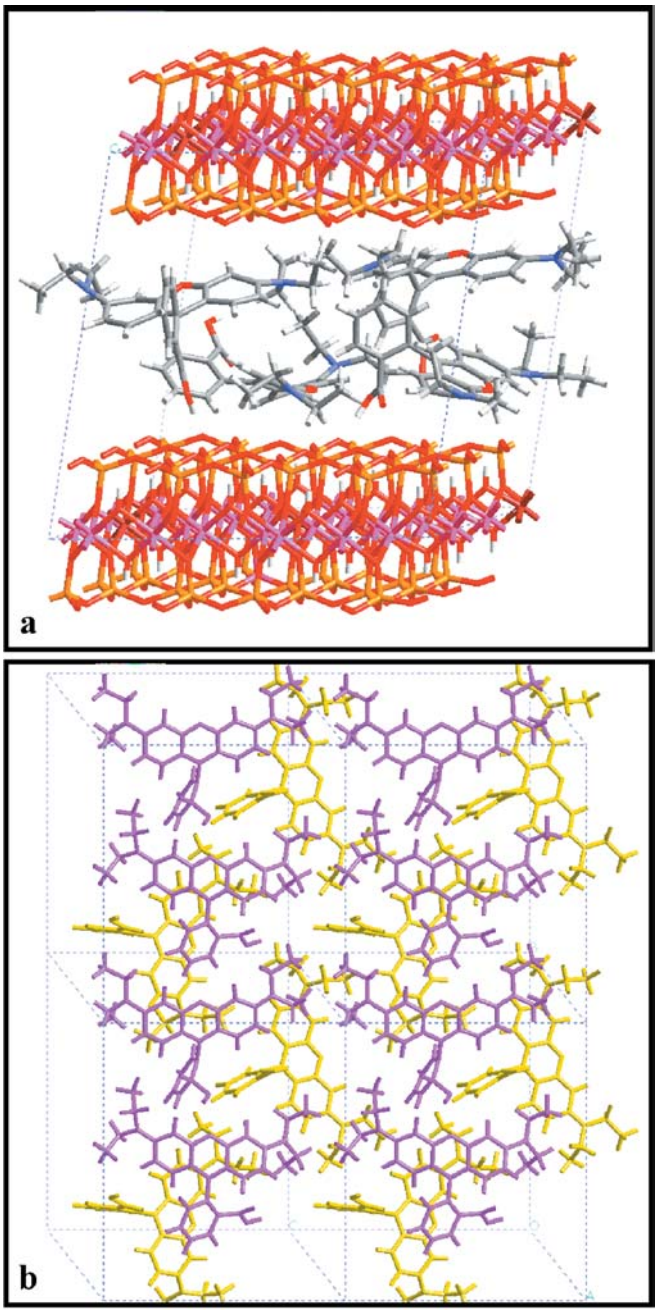

Fig. 5 **a** Side view of structure of the phase 18 Å, with bilayer arrangement of monomers (model 6 in Table 2). **b** Top view of structure of the phase 18 Å, with monomeric arrangement of [rhodamine B]$^{+}$ cations in two layers (lower layer *yellow*, upper layer *magenta*, silicate layer removed for clarity)

result of the Hendricks–Teller effect, we observe a peak shift and broadening of the 00*l* diffraction lines for the mixed phases. Another reason for the 00*l* broadening of the diffraction lines is the adsorption of water into the interlayer space, which causes fluctuations of the interlayer distance.

IR spectroscopy

Detailed analysis of the IR spectra for the host structure Na-montmorillonite, guest compound rhodamine B chloride and intercalate rhodamine B–montmorillonite confirmed the rigidity of the silicate layers and showed the changes in the IR spectra of rhodamine B in the intercalated structure. (Spectrometric identification was performed using. [24, 25]) First of all, comparing the spectrum of rhodamine B chloride and the intercalate in Fig. 2, one can observe the large broadening (smoothing) for the C=O stretching band in the carboxyl group at ~1700 cm^{-1} in the spectrum of the intercalate. Internal H-bonding reduces the carbonyl stretching frequency from 1720 cm^{-1} to 1665–1680 cm^{-1} and the smoothing of this band indicates orientational disorder of the carboxyl groups. The same effect of carboxyl disorder can be observed in the case of the C–O–H in-plane bending at ~1413 cm^{-1} and in case of C–O stretching at ~1300 cm^{-1}, this band almost disappears in the spectrum of intercalate.

The changes in the absorption bands corresponding to the aromatic rings are also evident in the spectrum of intercalate. As one can see in Fig. 2, there is a significant broadening (smoothing) of the bands corresponding to: (i) the in-plane bending of the ring C–H bonds in the region 1000–1300 cm^{-1}, (ii) the out-of-plane bending of the ring C–H bonds at ~ 675–900 cm^{-1} and (iii) the skeletal vibrations involving carbon–carbon stretching within the ring at ~ 1585–1600 cm^{-1} and 1400–1500 cm^{-1}. These changes in band profiles confirm the irregular positioning of the rhodamine B cations with respect to the silicate layers, the intramolecular rotations of the rhodamine B cations and a possible distortion of the xanthene part of the rhodamine B cation in the intercalate.

Results of modeling

A series of 80 initial models was investigated with various initial arrangements of monomers and dimers, with and without interlayer water. The molecular mechanics and dynamics simulations, carried out for the series of 80 initial models, result in two types of interlayer structure with the basal spacing 18.1 Å (phase 18 Å) and ~23 Å (phase 23 Å). The two phases differ significantly in the interlayer structure, but they exhibit certain common features:

- No regularly ordered positions of the rhodamine B anchored to the silicate layers were found, either for phase 18 Å or for 23 Å.
- Intramolecular rotation about the xanthene–amine bonds was observed in both phases. However, the change from the planar to pyramidal arrangement of the xanthene-diethylamine double bond is stronger for the phase 18 Å. The average departure from planarity for the phase 18 Å is ~29° and for the phase 23 Å about 21°. The presence of interlayer water slightly

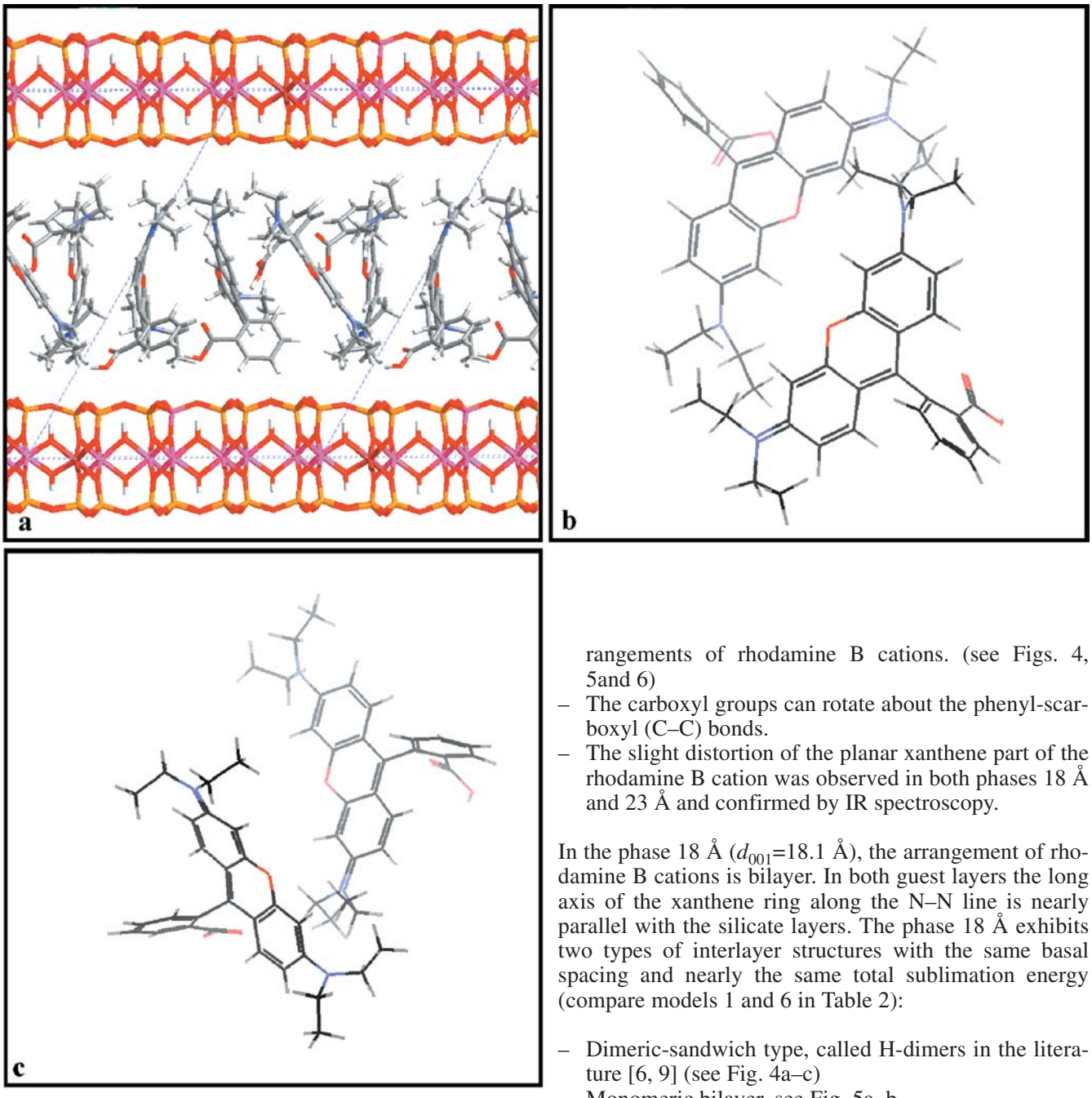

Fig. 6 **a** Side view of the phase 23 Å structure with monolayer arrangement of guests [rhodamine B]$^+$ (model 8 in Table 2). **b** Detailed view of the head-to-tail sandwich type of dimer occurring in the phase 23 Å. **c** Detailed view of the head-to-tail J- dimer occurring in the phase 23 Å

increases the departure from planarity, depending on the water content.
– The carboxyphenyl rings are perpendicular to the xanthene plane in the rhodamine B cation minimized in vacuum (see Fig. 3). In the interlayer space of montmorillonite, the phenyl rings may rotate about the xanthene–phenyl bonds in both phases and in all arrangements of rhodamine B cations. (see Figs. 4, 5and 6)
– The carboxyl groups can rotate about the phenyl-scarboxyl (C–C) bonds.
– The slight distortion of the planar xanthene part of the rhodamine B cation was observed in both phases 18 Å and 23 Å and confirmed by IR spectroscopy.

In the phase 18 Å (d_{001}=18.1 Å), the arrangement of rhodamine B cations is bilayer. In both guest layers the long axis of the xanthene ring along the N–N line is nearly parallel with the silicate layers. The phase 18 Å exhibits two types of interlayer structures with the same basal spacing and nearly the same total sublimation energy (compare models 1 and 6 in Table 2):

– Dimeric-sandwich type, called H-dimers in the literature [6, 9] (see Fig. 4a–c)
– Monomeric bilayer, see Fig. 5a, b

The H-dimeric arrangement is illustrated in Fig. 4a (a side view of the structure). In H- dimers, the rhodamine B cations interact with each other via the carboxyl groups. A detailed view of the H-dimer is shown in Fig. 4b. One can see the carboxyl groups pointing at the oxygen atom in the xanthene ring of the neighboring rhodamine B cation. It is also evident from Fig. 4b that the double xanthene=amine bonds of the two cations in the dimer are oriented in the same direction (head-to-head arrangement). Inclusion of water molecules into the interlayer space of the phase 18 Å leads to an increase of the total sublimation energy, as one can see in Table 2. That means the sorption of water is very probable. The

Table 2 Summary of the modeling results. Basal spacing and the total sublimation energy for the phases 18 Å and 23 Å with various arrangements of guests and with variable water content. Water content and the values of the total sublimation energy are related to one supercell 3*a*×2*b*×1*c*

Phase	Model no.	Structure	Number of water molecules in one supercell	Basal spacing d_{001} (Å)	Total subl. energy per one supercell (kcal mol^{-1})
18 Å	1	H-dimer	No water	18.1	876
18 Å	2	H-dimer	4	18.1	1052
18 Å	3	H-dimer	8	18.1	1133
18 Å	4	H-dimer	16	18.1	1425
18 Å	5	H-dimer[a]	32[a]	22.4[a]	3003[a]
18 Å	6	Monomers bilayer	No water	18.1	842
18 Å	7	Monomers bilayer	8	18.1	1030
23 Å	8	Monomers–dimers monolayer	No water	21–25	630–790
23 Å	9	Monomers–dimers monolayer	16	22.4	1491

[a] Prevailing water positions between the silicate layer and guest layer

increasing water content up to 16 water molecules per supercell 3*a*×2*b*×1*c* with two H-dimers does not change the basal spacing 18.1 Å (see Table 2), as there is a lot of empty space between the rhodamine B cations. Model 4 with 16 water molecules per supercell 3*a*×2*b*×1*c* is shown in Fig. 4c. Model 5 with 32 water molecules per one supercell exhibits an increase of basal spacing up to 22.4 Å and a large increase of the total sublimation energy per supercell (see Table 2). In contrast to models 2, 3 and 4, water molecules in model 5 reside mostly between the silicate and the guest layer. This effect of hydration explains the asymmetric broadening of the 001 diffraction line of the phase 18 Å in Fig. 1b. This phase 18 Å with the H-dimeric arrangement arises for intercalation solutions with high guest concentrations (see Table 1), i.e. with a strong tendency to dimerization.

The monomeric arrangement of rhodamine B cations in the phase 18 Å obtained from the modeling is shown in Fig. 5a, b. Figure 5a shows a side view of the structure, and the structure of the guests layers is shown in Fig. 5b from above (silicate layers were removed in Fig. 5b for clarity; the lower guest layer *yellow* and the upper guest layer *magenta*). Models 6 and 7 in Table 2 represent this structure, where only small interactions between the monomers occur. As one can see, the basal spacing is the same as in case of the H-dimeric arrangement, 18.1 Å. The total sublimation energy is slightly lower in comparison with model 1. The effect of hydration for the bilayer monomeric structure is the same as in case of the H-dimeric structure described above. The existence of this monomeric arrangement is a very important result of the modeling, as it can explain the presence of the phase 18 Å in the samples prepared from intercalation solutions with very low guest concentrations, i.e. with monomeric guest species.

The phase 23 Å was observed using intercalation solutions with very low concentrations of guests with prevailing monomeric arrangements. Modeling of the monomeric arrangement in the interlayer space of montmorillonite led to: (i) the bilayer arrangement (phase 18 Å) described above and (ii) to the monolayer arrangement of tilted monomers with a basal spacing within 21–25 Å, which we denoted as "phase 23 Å". An example of this structure is shown in Fig. 6a. In this phase 23 Å, the rhodamine B cations are tilted to the silicate layers. The tilting angles are in the range 40–60°. This wide range of positions and orientations of the rhodamine B cations in the interlayer results in disorder and strain in the interlayer space, which is intensified by the presence of interlayer water and leads to large fluctuations of the basal spacing. In this structure, the interactions between the monomers are stronger than in the bilayer phase 18 Å. In the phase 23 Å, a mixture of monomers and dimers was found in the interlamellar space. The two types of head-to-tail dimer found in this structure are illustrated in Fig. 6b and c. The dimer in Fig. 6b is the head-to-tail sandwich type (note the position of the single and double xanthene–amine bonds). On the other hand, the head-to-tail dimer in Fig. 6c is the so-called J-dimer described in the literature. [6, 9] It is evident that the J-dimer allows a higher degree of aggregation in the interlamellar space of montmorillonite. Insertion of water molecules into the interlayer structure of the phase 23 Å leads to fluctuations of the basal spacing, within the range 21–25 Å.

Table 3 Comparison of the mutual intermolecular interaction energy between monomers in three types of dimers (interaction energy includes the non-bond, i.e. the van der Waals and electrostatic contributions)

Dimer type	H-dimer	Head-to-tail sandwich	J-dimer
Interaction energy (kcal)	23.5	9.3	5.1

Conclusions

The present results have revealed in detail the structure of montmorillonite intercalated with [rhodamine B]$^+$ cations and the mechanism of the intercalation process.

Two structural phases were observed by X-ray diffraction and modeling: (i) phase 18 Å with a bilayer arrangement of guests and (ii) phase 23 Å with a monolayer arrangement of guests. In both phases, the coexistence of monomeric and dimeric arrangement is possible. Three types of dimer have been observed using molecular mechanics and molecular dynamics simulations: H-dimer (head-to-head), head-to-tail sandwich and head-to-tail J-dimer. Comparing their mutual non-bond interaction energy (see Table 3), one can see that the H-dimers are most stable.

The present modeling results agree with the X-ray diffraction measurements. Both methods revealed the existence of the two phases, where the basal spacing obtained from modeling agrees with the experimental value. The results of modeling also help to explain the structural disorder and its effect on the diffraction pattern (line shift and line broadening). IR spectroscopic measurements also corroborate the modeling results. The intramolecular rotational disorder obtained from modeling has a corresponding response in the IR spectra of the intercalate. As a result of this intramolecular rotation, we can observe the broadening of the C=O and C–O stretching and C–O–H in-plane bending bands. The broadening of bands corresponding to the in-plane and out-of-plane bending of the ring C–H bonds and of the skeletal vibrations involving carbon–carbon stretching within the ring indicates slight distortions of the xanthene ring, which have been obtained by modeling.

Acknowledgements This work was supported by the Grant Agency of the Czech Republic, grant no GAČR 205/02/0941, and by the Ministry of Education of the Czech Republic, grant no MSM 113200001.

References

1. Endo T, Nakada N, Sato T, Shimada M (1988) J Phys Chem Solids 49:1423–1428
2. Estévez MJT, Arbeloa FL, Arbeloa TL, Arbeloa IL (1995) J Colloid Interface Sci 171:439–445
3. Estévez MJT, Arbeloa FL, Arbeloa TL, Arbeloa IL (1994) J Colloid Interface Sci 162:412–417
4. Arbeloa FL, Martínez JMH, Arbeloa TL, Arbeloa IL (1998) Langmuir 14:4566–4573
5. Ogawa M, Aono T, Kuroda K, Kato C (1993) Langmuir 9:1529–1533
6. Chaudhuri R, Arbeloa FL, Arbeloa IL (2000) Langmuir 16:1285–1291
7. Estévez MJT, Arbeloa FL, Arbeloa TL, Arbeloa IL (1993) Langmuir 9:3629–3634
8. Arbeloa FL, Estévez MJT, Arbeloa TL, Arbeloa IL (1995) Langmuir 11:3211–3217
9. Arbeloa FL, Chaudhuri R, Arbeloa TL, Arbeloa IL (2002) J Colloid Interface Sci 246:281–287
10. Ogawa M, Wada T, Kuroda K (1995) Langmuir 11:4598-4600
11. Lagaly G, Weiss A (1969) Determination of the layer charge in mica-type layer silicates. In: Heller L (ed) Proceedings of the International Clay Conference, Tokyo, vol 1. Israel University Press, Jerusalem, pp 61–80
12. Lagaly G (1986) Solid State Ionics 22:43–51
13. Lerf A (2000) Intercalation compounds in layered host lattices: supramolecular chemistry in nanodimensions. In: Nalwa HS (ed) Handbook of nanostructured materials and nanotechnology, vol 5. Academic Press, New York, pp 1–166
14. Breu J, Raj N, Catlow CRA (1999) J Chem Soc Dalton Trans 6:835–845
15. Breu J, Catlow CRA (1995) Inorg Chem 34:4504–4510
16. Cerius2 forcefield-based simulations (1997) Molecular Simulations Inc, San Diego
17. Tsipursky SJ, Drits VA (1984) Clay Miner 19:177–193
18. Méring J, Oberlin A (1967) Clays Clay Miner 27:3–18
19. Karasawa A, Goddard III WA (1989) J Phys Chem 93:7320–7327
20. Rappé AK, Goddard III WA (1991) J Phys Chem 95:3358–3363
21. Rappé AK, Casewit CJ, Colwell KS, Goddard III WA, Skiff WM (1992) J Am Chem Soc 114:10024–10035
22. Berendsen HJC, Postma JPM, van Gunsteren WF, DiNola A, Haak JR (1984) J Chem Phys 81:3684–3690
23. Hendricks S, Teller E (1942) J Chem Phys 10:147–167
24. Silverstein RM, Bassler GC, Morrill TC (1991) Infrared spectrometry. In: Sawicki D (ed) Spectrometric identification of organic compounds. Wiley, New York, pp 91–132
25. Farmer VC (1974) The layer silicates. In: Farmer VC (ed) The infrared spectra of minerals, chapter 15. Mineralogical Society, London, pp 331–363